The Journal of Chemical Physics

RESEARCH ARTICLE | MAY 08 2023

Complexities in the structural evolution with pressure of water–ammonia mixtures

Selene Berni; Demetrio Scelta ✉; Samuele Fanetti; ... et. al

J. Chem. Phys. 158, 184302 (2023)
https://doi.org/10.1063/5.0150639

AIP Publishing

The Journal of Chemical Physics ARTICLE scitation.org/journal/jcp

Complexities in the structural evolution with pressure of water–ammonia mixtures

Cite as: J. Chem. Phys. 158, 184302 (2023); doi: 10.1063/5.0150639
Submitted: 15 March 2023 • Accepted: 24 April 2023 •
Published Online: 8 May 2023

Selene Berni,[1] Demetrio Scelta,[2,a),b)] Samuele Fanetti,[2,b)] and Roberto Bini[3,b),c)]

AFFILIATIONS

[1] LENS, European Laboratory for Non-linear Spectroscopy, Via N. Carrara 1, I-50019 Sesto Fiorentino, Firenze, Italy
[2] ICCOM-CNR, Istituto di Chimica dei Composti OrganoMetallici, Via Madonna del Piano 10, I-50019 Sesto Fiorentino, Firenze, Italy
[3] Dipartimento di Chimica "Ugo Schiff," Università di Firenze, Via della Lastruccia 3, I-50019 Sesto Fiorentino, Firenze, Italy

[a)] **Author to whom correspondence should be addressed:** scelta@lens.unifi.it
[b)] **Also at:** LENS, European Laboratory for Non-linear Spectroscopy, Via N. Carrara 1, I-50019 Sesto Fiorentino, Firenze, Italy.
[c)] **Also at:** ICCOM-CNR, Istituto di Chimica dei Composti OrganoMetallici, Via Madonna del Piano 10, I-50019 Sesto Fiorentino, Firenze, Italy.

ABSTRACT

The structural evolution with pressure of icy mixtures of simple molecules is a poorly explored field despite the fundamental role they play in setting the properties of the crustal icy layer of the outer planets and of their satellites. Water and ammonia are the two major components of these mixtures, and the crystal properties of the two pure systems and of their compounds have been studied at high pressures in a certain detail. On the contrary, the study of their heterogeneous crystalline mixtures whose properties, due to the strong N–H···O and O–H···N hydrogen bonds, can be substantially altered with respect to the individual species has so far been overlooked. In this work, we performed a comparative Raman study with a high spatial resolution of the lattice phonon spectrum of both pure ammonia and water–ammonia mixtures in a pressure range of great interest for modeling the properties of icy planets' interiors. Lattice phonon spectra represent the spectroscopic signature of the molecular crystals' structure. The activation of a phonon mode in plastic NH_3-III attests to a progressive reduction in the orientational disorder, which corresponds to a site symmetry reduction. This spectroscopic hallmark allowed us to solve the pressure evolution of H_2O–NH_3–AHH (ammonia hemihydrate) solid mixtures, which present a remarkably different behavior from the pure crystals likely to be ascribed to the role of the strong H-bonds between water and ammonia molecules characterizing the crystallites' surface.

I. INTRODUCTION

Water, methane, and ammonia are the major constituents of the ices present in the mantles of icy planets within and outside the solar system.[1–8] The composition, structure, and properties of these planets' interiors can be constrained by models that rely on laboratory studies directed to clarify the properties of the single components, and those of their mixtures, under the pressure and temperature conditions characterizing these hardly accessible environments. Methane–water mixtures have extensively been studied because of the clathrate hydrate formation and of the relevance they have in understanding the origin and persistence of methane on Titan's surface.[9–14] Water–ammonia mixtures are definitely less studied and limited to relatively lower pressures, although they are more relevant for the description of icy planets. Different stoichiometric crystalline hydrates have been identified: ammonia monohydrate (AMH, H_2O:NH_3), ammonia hemihydrate (AHH, H_2O:$2NH_3$), and ammonia dihydrate (ADH, $2H_2O$:NH_3). Among them, AMH is definitely the most studied with three out of five low temperature crystal phases solved.[15,16] Two other peculiar AMH phases form above 270 K. At 6.5 GPa, a new phase (AMH-VI) has been identified, where water and ammonia randomly occupy the sites of a *bcc* lattice giving rise to what is called a disordered molecular alloy (DMA),[17] stable at least up to 40 GPa.[18] Partial ionization has experimentally been proven for this phase above 7.4 GPa and up to 40 GPa by spectroscopic and x-ray diffraction experiments,[19] thus

confirming the predictions of a transformation into an ionic solid made by NH_4^+ and OH^- in the proximity of 10 GPa.[20–22] Recently, another AMH plastic phase (AMH-VII) has been identified above 3.6 GPa and 324 K[23] possessing the same structure as AMH-VI and also composed of ions and molecules.[24] The relevance of these hydrates mainly lies in the formation of ionic phases under milder conditions than the extreme pressures and temperatures required for pure systems.[25–28] Ionic crystals have also been predicted for AHH, which, peculiarly, consists of NH_4^+ cations and O^{2-} anions above 65 GPa.[29]

Preliminary to the study of complex mixtures, which better reflect the real composition of icy planets,[2] a precise characterization of the pure components and of their simplest mixtures is also mandatory. Among ammonia hydrates, AMH and ADH have primarily been investigated because water is by far the most abundant between the two in the primitive nebula.[30,31] However, the relevance of AHH to planetary modeling was raised by the decomposition of AMH in AHH phase-II and water ice at about 3.5 GPa.[16] The AHH-II directly forms from 2:1 ammonia–water solutions upon room temperature compression above 3.5 GPa and transforms above 19 GPa to the AHH-DMA structure.[32] This order–disorder transition and the melting/crystallization of AHH-DMA have been carefully characterized also at lower pressures and high temperatures by neutron and x-ray diffraction experiments.[18]

One of the common problems encountered in the interpretation of spectroscopic and diffraction data of hydrates under high-pressure conditions is represented by their coexistence in the sample with pure components. This occurrence, hard to avoid, is due to the enrichment of some of the elements during the loading or simply to demixing. Actually, this can also be an opportunity to have an icy sample compliant with those found in nature, where extended pure phase segregation is surely quite rare. In this work, we have studied 2:1 water–ammonia mixtures under moderate pressures (≤15 GPa) by Raman spectroscopy, finding some peculiar results that suggested us to reinvestigate the low-pressure phase diagram of ammonia and specifically what concerns the plastic phase III. Below 12 GPa, ammonia presents four different solid phases.[33] Phase I (cubic $P2_13$) is stable at low temperatures (≤220 K) up to about 2 GPa. Between 220 and 260 K, the compression of the liquid leads to the crystallization in an hcp structure (phase II $P6_3/mmc$), whereas at higher temperatures, another face-centered cubic phase (III $Fm\bar{3}m$) is obtained. Both phases II and III are characterized by rotational disorder (plastic phases). The orthorhombic phase IV ($P2_12_12_1$) is obtained by compressing all three low-pressure crystals, with the transition occurring at 3.6 GPa at ambient temperature.[34–37]

In this paper, we report an experimental high-pressure Raman study of pure ammonia and 2:1 water–ammonia mixtures between 240 and 380 K up to 15 GPa. The transition line between the ammonia crystal phases II and III has been determined together with the evolution of the lattice phonons spectrum through the II–III–IV phases. The activation of a Raman active phonon in phase III has been interpreted on the basis of a progressive reduction in the orientational disorder characterizing this phase. As far as the mixture is concerned, the crystallization of water and AHH-II takes place at considerably higher pressures in the regions where they are minor components, whereas NH_3-III survives in the whole investigated pressure range inhibiting the formation of phase IV, which is never observed at least up to 15 GPa and between 300 and 380 K. These observations evidence important interactions in the crystal phase, presumably due to strong H-bonds between water and ammonia molecules, which result in a kinetic control of the phase transitions.

II. EXPERIMENTAL

The high pressure was generated through membrane diamond anvil cells (mDAC) equipped with IIas diamonds with 400 μm culet diameter. The sample was contained sideways by rhenium gaskets, and ruby chips were added to the sample chamber to monitor the sample pressure by the ruby fluorescence method.[38] The samples of pure ammonia were prepared by the spray-loading technique as described elsewhere.[39] The DAC was put into a sealed box and cooled down by liquid nitrogen. Ammonia (Sapio, purity 99.99%) was sprayed onto the diamonds at a temperature maintained around 100 K under a heavy flow of gaseous nitrogen to avoid the condensation of air components, such as water or CO_2. The samples containing the ammonia hydrates were prepared depositing a small drop of 33% in weight ammonia/water solution into the DAC sample chamber at ambient temperature. The DAC was then closed and pressurized. The Raman measurements were performed with a 660 nm diode laser as an excitation source. In our Raman setup, we used a back-scattering geometry and, for ambient temperature experiments, a long working distance 20× Mitutoyo micro-objective, while in the low temperature measurements, the use of a cryostat dictated the employment of a 5× Mitutoyo micro-objective. In ambient and high temperature experiments, the spatial resolution on the sample was about 3 μm.[40] Spectra were collected using an Acton/SpectraPro 2500i monochromator equipped with holographic super notch filters and a CCD detector (Princeton Instruments Spec-10:100BR) with a resolution of 1 cm^{-1}.[40] The low temperature experiments were carried out using a helium closed-cycle cryostat, whereas for the high temperature measurements, the DAC was resistively heated under vacuum. The temperature was determined by a silicon diode placed very close to one of the diamonds, with a nominal accuracy of 1 K. Pressure was measured by the shift of the ruby fluorescence wavelength corrected for temperature.[41]

III. RESULTS

A. Pure ammonia

Upon compression, ammonia crystallizes at ambient temperature above 1.0 GPa in a cubic structure indicated as phase III. The structure was solved as ($Fm\bar{3}m$) (O_h^5) with an orientationally disordered molecule in the primitive cell (site symmetry O_h).[45] The Raman spectrum of this phase resembles that of the liquid in the N–H stretching region, and no Raman active lattice modes are observed, as expected, according to the crystal symmetry[33] (see the top correlation diagram in Table I). However, the appearance of a strong low frequency Raman band above 2 GPa, i.e., before the transition to phase IV (~3.8 GPa), was mentioned by the same authors who proposed as a possible explanation of this occurrence an inaccurate determination of the II–III phase boundary.[33] In the first experiment we performed, the pressure after the loading was above

TABLE I. Correlation diagrams for the lattice phonon modes and expected Raman and IR activity. The diagrams for the cubic structures proposed by Von Dreele and Hanson[45] according to x-ray diffraction experiments are reported in the top and central panels. Acoustic phonons are indicated as *ac*. The preferred structure (top) does not envisage phonon activity, whereas that corresponding to the central panel expects one librational Raman band. The third correlation diagram (bottom), the one we suggest, corresponds to the structure proposed by Von Dreele and Hanson but with a lower site symmetry: Here, a translational Raman active mode is expected.

Site	Factor group	Activity
O_h	O_h^5 $(Fm\bar{3}m)$	
T_{1u} (T_x, T_y, T_z)	T_{1u}	*ac* IR (x,y,z)
T_{1g} (R_x, R_y, R_z)	T_{1g}	...
Site	Factor group	Activity
T_h	T_h^3 $(Fm\bar{3})$	
T_g (R_x, R_y, R_z)	T_g	R (xz, yz, xy)
T_u (T_x, T_y, T_z)	T_u	*ac* IR (x, y, z)
Site	Factor group	Activity
T_d	O_h^5 $(Fm\bar{3}m)$	
T_1 (R_x, R_y, R_z)	T_{1g}	...
	T_{2u}	...
T_2 (T_x, T_y, T_z)	T_{2g}	R (xz, yz, xy)
	T_{1u}	*ac* IR (x,y,z)

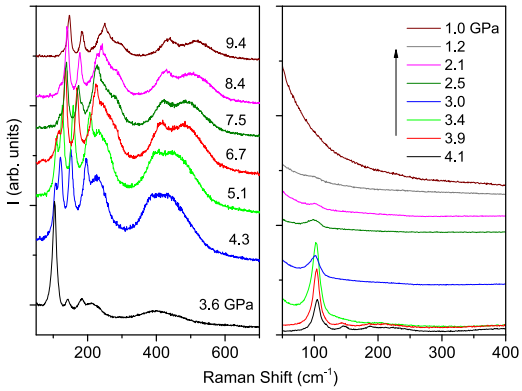

FIG. 1. Lattice phonon Raman spectra of ammonia NH_3-III and NH_3-IV. Left panel: re-compression after having obtained phase III (black trace) through the decompression of phase IV, which was produced in the loading. The spectra at, and above, 4.3 GPa are relative to phase IV. Right panel: decompression in phase III down to the melting (1 GPa).

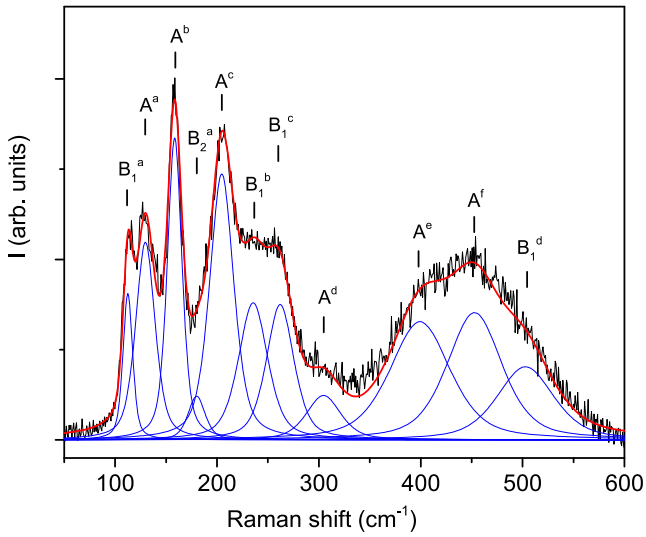

FIG. 2. Deconvolution of the lattice phonon spectrum measured in NH_3-IV at 5.1 GPa. The assignment adopted is from Ref. 35.

5 GPa showing the typical spectrum of phase IV as we will discuss in the following. The decompression below the III–IV phase transition pressure revealed a very intense peak around 100 cm^{-1} not ascribable to phase IV (see the black trace in the left panel of Fig. 1). The sample was compressed again up to about 10 GPa, and around 4 GPa, we observed the formation of phase IV. The following decompression showed again the appearance of a low frequency strong peak at about 4 GPa, confirming that the peak observed at 3.6 GPa was not related to phase IV. The entire compression–decompression process, relative to the lattice phonon region, is shown in Fig. 1. Importantly, the intensity of the phase III phonon considerably decreases with releasing pressure (right panel of Fig. 1), while, simultaneously, an intensification of the Rayleigh wings is observed, suggesting a liquid-like contribution to the scattering.

As far as phase IV is concerned, the spectrum was deconvoluted as shown in Fig. 2 and the pressure shift of the lattice phonon bands was determined and is reported, together with that of phase III, in Fig. 3. The assignment reported in Fig. 2 follows that from Ref. 35 where the lattice modes were measured by Raman spectroscopy at temperatures below 80 K. Despite the large bandwidths due to the high temperature, we succeeded in identifying most of the expected Raman active lattice bands, including the lowest in frequency (112 cm^{-1} at 5.7 GPa), not reported by Ninet *et al.*[35] (their spectra were limited to 130 cm^{-1}) but expected, according to their DFT calculations, at 110 cm^{-1} at 6.3 GPa (0 K).

The pressure shift of the phonon modes reported in Fig. 3 highlights the III–IV phase transition, which is marked by a clear discontinuity (upper panel) in the frequency values of the lowest peak (B_1^a) of phase IV and the one characteristic of phase III. In addition, the peak of phase III is remarkably stronger than that of phase IV when the transition is crossed in decompression.

In order to verify the effective presence of a phonon band in the pressure range characteristic of phase III, we compressed another sample starting from the liquid phase without reaching phase IV. The phonon band appeared only above 2 GPa, in remarkable agreement with the observation made by Gauthier *et al.*,[33] while the crystallization took place around 1 GPa. This band intensifies with increasing pressure and shows perfect reversibility in decompression (see Fig. 4). Interestingly, the intensity of the phonon peak of phase III is much larger when the sample is decompressed from phase IV than when phase III is produced upon compression of the liquid.

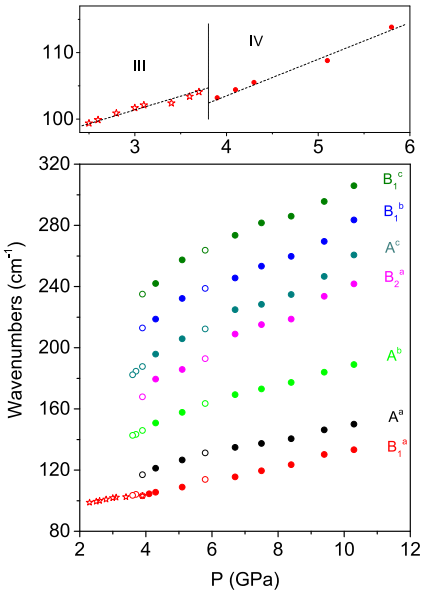

FIG. 3. Pressure shifts of the Raman active lattice modes measured in NH_3-III (stars) and NH_3-IV (circles). The full and empty symbols correspond to the data acquired in compression and decompression, respectively. The assignment is from Ref. 35. In the upper panel, an expanded view of the pressure shift relative to the lowest phonon of phase IV and the one of phase III is reported to highlight the frequency discontinuity. The pressure and peak frequency uncertainties are of the same size as the symbols employed in the top panel. The dashed lines are a guide to the eye.

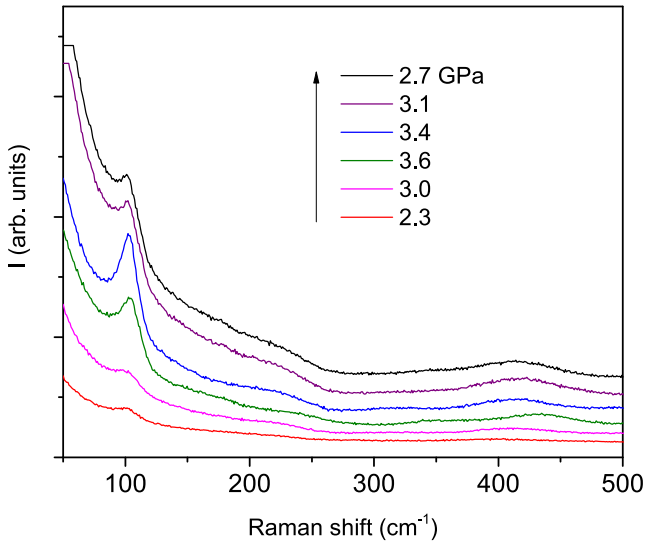

FIG. 4. Compression–decompression evolution of the lattice Raman spectrum of NH_3-III. The spectra have been acquired in the order shown by the arrow in the inset.

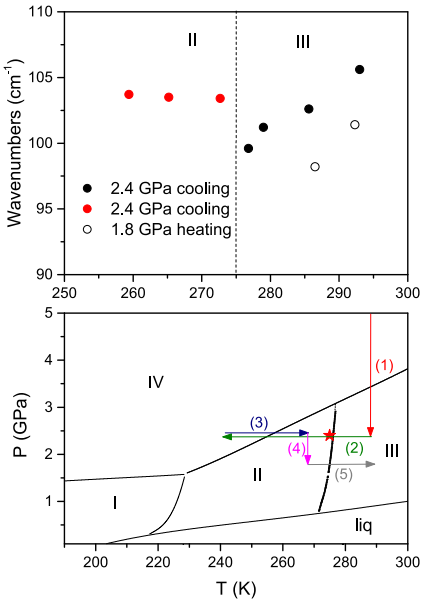

FIG. 5. Lower panel: P–T path followed to detect the II–III phase boundary. The numbers indicate the sequence of the different P–T steps. The red star corresponds to the P–T condition where we detected the II–II phase transition (data in the upper panel). Upper panel: Temperature shift of the lattice phonons of phases III and II measured at 2.4 GPa on cooling (full symbols). The empty symbols refer to the measurements performed on heating at 1.8 GPa after having recovered phase III. The peak frequency uncertainties are of the same size as the symbols.

The appearance of the lattice phonon band above 2 GPa was speculated to be due to phase II because of an inaccurate placement of the II–III phase transition.[33] For this reason, we first produced phase III by decompressing phase IV in order to have a quite strong phonon band, then phase III was isobarically cooled at 2.4 GPa acquiring spectra both in the lattice phonons and in the N–H stretching regions. A single phonon is observed down to 247 K, where the transition to phase IV is revealed by the sudden appearance of its complex phonon spectrum extending from 90 to 200 cm^{-1}. However, a clear discontinuity and the slope change of the phonon frequency are observed at 275 K (see Fig. 5) in perfect agreement with the P–T value expected for the II–III phase transition on the basis of the phase diagram reported by Gauthier *et al.*[33] The IV–II transition was not observed when we heated again the sample also reducing the pressure to 1.8 GPa. We only recovered the characteristic phonon of phase III when we reached 286 K, i.e., well inside the phase III domain. The presence of a Raman active lattice phonon in phase III is, therefore, demonstrated, thus questioning the current structural assignment that envisages neither Raman nor IR active lattice modes.

B. The 2:1 water-ammonia mixture

The 2:1 water–ammonia mixture has been compressed starting in the liquid phase (0.8 GPa) up to 14.2 GPa. The sample appearance changed a lot during compression as shown in Fig. 6. The crystallization pressure of ammonia does not change in the mixture being observed at 1.25 GPa through the appearance of the phase III phonon band at about 100 cm^{-1}. At 2.7 GPa, the typical phonon bands of ice VI around 200 cm^{-1} are observed, thus attesting to water solidification.[42] This pressure is much higher than that at

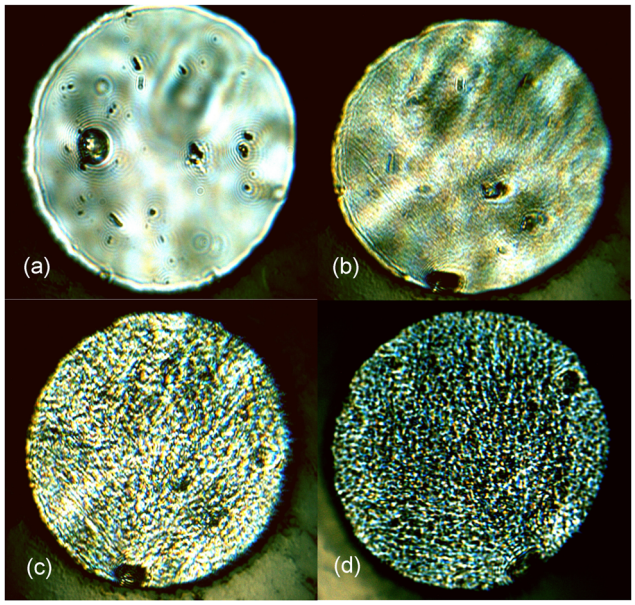

FIG. 6. Images of the water–ammonia samples acquired along the compression of the mixture at: (a) 1 GPa, both components are in the liquid phase; (b) 2.5 GPa, the changes in the sample appearance are due to the ammonia crystallization; (c) 3.0 GPa, all the sample is solid; (d) 13.4 GPa.

which water crystallizes into phase VI in the pure system (~1 GPa). The transformation of ice VI into ice VII also occurs at about 1 GPa above (~3 GPa) compared to in pure water. This sequence is shown in Fig. 7. The formation of ice-VII coincides with a consistent modification of the sample appearance that changed from being smooth and homogeneous to assume an evident texture [see panel (c) of Fig. 6]. Despite an apparent homogeneity of the sample, Raman mapping showed clear differences in the sample composition with portions richer in ice VII and ammonia hydrate and others in pure NH_3-III. A selection of spectra measured in the NH_3-rich portion along the compression and decompression cycles is shown in Fig. 8. In the lattice phonon region (left panel), the phonon band characterizing NH_3-III is the only one present below 7 GPa and this is quite surprising because in pure ammonia the formation of phase IV takes place at about 4 GPa. Remarkably, this peak, and then phase III, survives in the entire explored pressure range (up to 14 GPa) and along the following decompression, whereas the phonon spectrum of phase IV (see Figs. 1 and 2) is never observed. The broader band appearing at about 7 GPa at 300 cm^{-1} is due to ice VII,[43] and it is observable along the entire compression–decompression cycle. Around 9 GPa, new bands enrich the spectrum: a doublet at 144 and 156 cm^{-1} and a broader and asymmetric band at 223 cm^{-1}. However, all these features are well visible in Fig. 8 only at 11.5 GPa. These peaks nicely agree with the data reported for AHH-II.[32] Nevertheless, upon decompression, the spectral signatures of AHH-II disappear around 6–7 GPa, i.e., 3–4 GPa above what is reported in the literature.[18] In the stretching region (right panel of Fig. 8), the weak Raman bands of NH_3-III are the only ones observed up to 6–7 GPa. Above this pressure, the bands of ice VII dominate the spectrum exhibiting the characteristic red-shift on compression.[43] These spectra also confirm the missed formation of NH_3-IV because the strong sharp peak lying just below 3400 cm^{-1} characterizing the N–H stretching region in phase IV (see Fig. 9) is never detected.

The regions where ammonia hydrate and ice VII dominate can be quite easily identified by the spectral differences both in the lattice and in the stretching region (see Fig. 10). The phonon spectrum measured at 2.6 GPa contains the phonon bands of NH_3-III and ice VI.[42] The formation of ice VII can be clearly identified by the

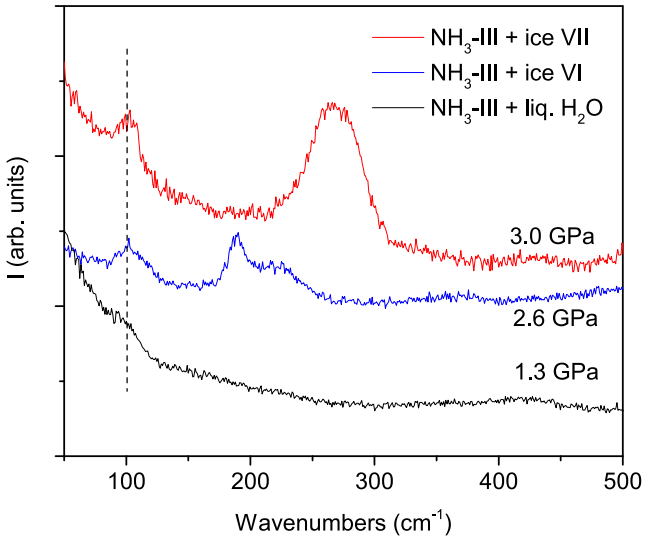

FIG. 7. Phonon spectra attesting for the crystallization of NH_3-III and ice VI, and for the following transition to ice VII. The dashed line indicates the phonon line of NH_3-III.

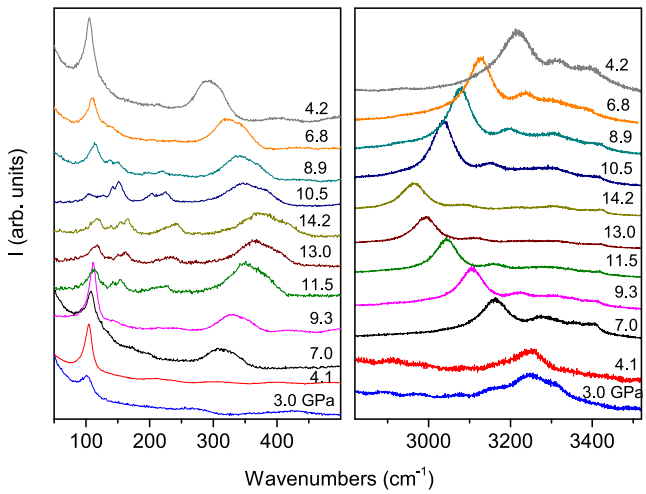

FIG. 8. Raman spectra measured upon compressing–decompressing the water–ammonia mixture in the NH_3-rich portion of the sample. Lattice phonons and O–H and N–H stretching regions are reported in the left and right panels, respectively.

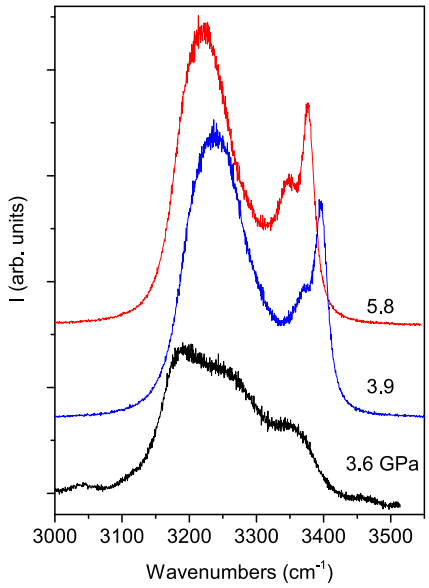

FIG. 9. Examples of Raman spectra measured in the N–H stretching region in NH_3-III (black trace) and NH_3-IV (blue and red traces).

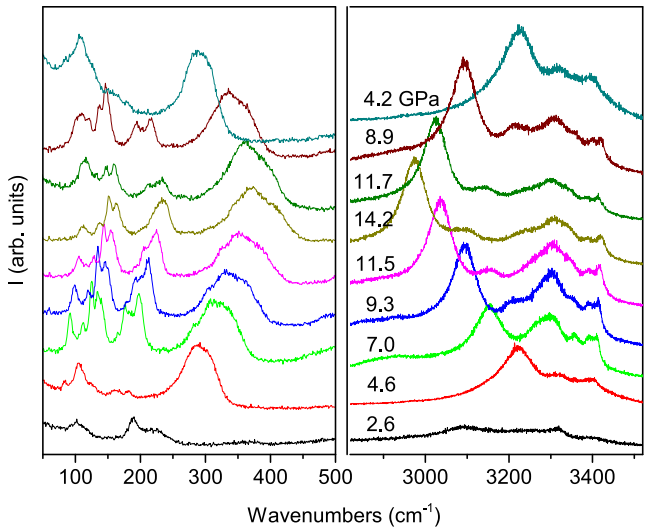

FIG. 10. Raman spectra measured upon compressing–decompressing the water–ammonia mixture in the AHH-rich portion of the sample. Lattice phonons and O–H and N–H stretching regions are reported in the left and right panels, respectively.

strong and broad band at 300 cm^{-1} which appears above 3 GPa. At 4.6 GPa, the lattice phonon spectrum is enriched with new bands ranging between 92 and 198 cm^{-1}. These bands intensify with pressure, making the identification at 7 GPa of at least nine peaks possible (see the deconvolution in Fig. 11). All the peaks are observable up to a maximum pressure of 14.2 GPa, nicely agreeing with the AHH literature data.[32,44] This behavior is perfectly

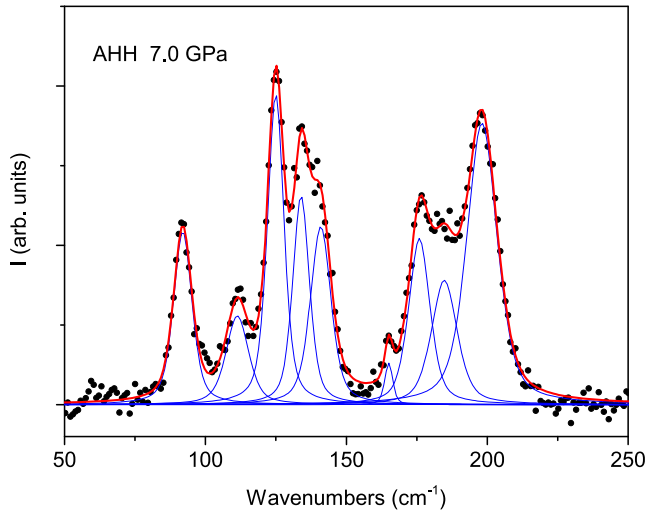

FIG. 11. Deconvolution of the lattice phonon spectrum of AHH-II measured at 7.0 GPa.

reversible in decompression, and below 5 GPa, the characteristic features of AHH-II disappear and the phonon spectrum of NH_3-III is again clearly observed. In addition, the stretching region confirms the local sample composition. Besides the strong O–H stretching band of ice VII, the characteristic spectral structure of AHH-II[32,44] is well visible above 7 GPa between 3200 and 3450 cm^{-1}.

IV. DISCUSSION

Two major issues emerge from this study: the inconsistency between the spectroscopic data and the structure so far proposed for NH_3-III, and the quite different high-pressure behavior of the mixture components with respect to the pure systems, an aspect of great importance for interpreting observations and model the composition of remote icy mixtures. Although already mentioned, but not discussed, by Gauthier *et al.*,[33] the observation of the Raman phonon in phase III is certainly an intriguing result of this study. According to the structure proposed by Dreele *et al.*,[45] phase III is cubic $(Fm\bar{3}m)$ (O_h^5) with one orientationally disordered molecule in the primitive cell (site O_h); therefore, neither Raman nor IR activity is expected in the lattice mode region (see the correlation diagram in Table I). The structure ultimately proposed by Dreele *et al.* was preferred to one of lower symmetry, $(F_m\bar{3})$ (T_h^3), on the basis of similarities with ammonia phase I and of the reflections' intensities.[45] The $(F_m\bar{3})$ (T_h^3) structure is compatible with the observation of a Raman active phonon since a T_g Raman active mode is expected in this case, corresponding to a triply degenerate librational mode (see Table I). As previously mentioned, the observation of this phonon was also reported by Gauthier *et al.*[33] who invoked a misplacement of the II–III phase boundary. However, the experiments we performed by isobarically cooling phase III clearly demonstrate that the phonon observed at ambient temperature is characteristic of this phase and it is not due to the presence of phase II. In all the experiments we performed, a reproducible

intensification/weakening of this mode with increasing/decreasing pressure is observed. In addition, a remarkably higher intensity of the phonon band is observed when phase III is obtained decompressing the fully ordered phase IV, thus indicating a clear dependence on density and likely on a pre-existing molecular ordering. As a matter of fact, the crystal density remarkably increases between 1 GPa, the crystallization pressure, and 2 GPa with a volume decrease of more than 11%, with a smoother reduction (about 5%) between 2 and 3 GPa.[45,46] This behavior parallels that reported for the plastic cubic (Pm3n) δ phase of nitrogen crystal upon lowering the temperature or increasing the pressure. In that case, the activation of an infrared active Davydov component of the ν_2 mode (stretching of the disk-like molecules) was reported,[47] and also, in that case, the intensity increased on cooling or on compression. This behavior was interpreted as due to the localization of the freely rotating disk-like molecules, i.e., to a progressive blocking of their rotational motion and then to a local symmetry reduction. Further support to a similar interpretation in the case of NH_3-III is given by the reproducible behavior of the low frequency part ($\nu \leq 100$ cm^{-1}) of the spectrum, which intensifies when the phonon intensity decreases and vice versa, thus revealing a continuous evolution toward a structure characterized by orientational disorder (liquid-like). We, therefore, favor a progressive reduction of the orientational disorder, corresponding to a site symmetry reduction (reported in the bottom correlation diagram of Table I from O_h to T_d), which accounts for both the activation of a Raman active lattice mode and the progressive reduction in the liquid-like contribution to the lower frequency portion of the spectrum.

Another important outcome of this study is related to the quite complex behavior of the water–ammonia mixture on increasing the pressure. Despite having a 2:1 water–ammonia composition, we detected in many different samples a very heterogeneous distribution of the three present crystalline species: water, ammonia, and AHH. In all the previous studies, the attention was generally focused on the crystalline hydrate phases (AMH, ADH, and AHH) characterization, neglecting the quite relevant effects on the pure systems. As a consequence, the exact spatial composition of the mixture is often overlooked or barely discussed. On the contrary, this study demonstrates that it is central for understanding the real environments where these species are encountered. Indeed, thermoelastic and transport properties strictly depend on density changes that are very consistent in phase transitions in the low-pressure regime of both pure systems and hydrates.[48] In addition, also an accurate knowledge of the melting pressure and temperature conditions is mandatory to highlight phenomena such as cryovolcanism, or the melt diffusion direction, upward or downward, which is dictated by the density contrast with the surrounding solid phases.[6] The latter issue is immediately addressed by the observation of the crystallization pressure of water, or at least of the formation of ice-VI, that shifts from 1 to 2.7 GPa, a pressure value where, in the pure system, ice-VII is the thermodynamically stable phase. An increase in the crystallization pressure is expected for a mixture, and for instance, it was observed in a 2.5 wt. % methanol solution, where the ice VI crystallization occurred at 1.3 GPa.[49] However, the sizable entity of the melting point shift in the present case is likely related to the high ammonia concentration. As a matter of fact, the ice crystallization should be preceded by the segregation of water clusters that can trigger the nucleation process. Water segregation in homogeneous fluid mixtures has been found to increase with pressure in water–methanol solutions,[50] but the extent and the conditions required are obviously also ruled by the nature and the concentration of the solute.

The explanation of the higher pressure values where the solid–solid transitions occur is more difficult. The ice VI-VII phase transition takes place around 3 GPa, therefore, 1 GPa higher than in pure ice, whereas, no differences were detected in the H_2O–CH_3OH mixture with respect to pure ice.[49] Also, the signatures of AHH-II, which is reported to form from the mixture around 3 GPa,[32] are observed here at different pressures depending on the environment. Indeed, AHH-II appears in compression around 4,6 GPa in the AHH/ice VII rich regions, and at much higher pressure, 11.5 GPa, in the NH_3-rich region. Consistently, in both regions, the hemihydrate decomposition is observed between 6 and 7 GPa, which is remarkably higher than expected.[18,32] However, the most surprising result is the missed observation, in the NH_3-rich regions, of NH_3-IV up to the maximum pressure reached in the experiment, roughly corresponding to the IV–V phase transition.[33]

In pure NH3, phase IV readily forms from phase III between 3.8 and 4 GPa. On the contrary, in the mixtures, we observe the persistence of NH3-III in the entire pressure interval, as attested by the phonon spectrum where the single Raman band characterizing phase III is observed in place of the rich phonon spectrum of phase IV. It is probably superfluous but worth recalling that the phonon spectrum represents the spectral signature of the crystal. The anomalies in the phase transition values and the missed observation of NH_3-IV can result from the strong interactions, primarily hydrogen bonds, within the variously composed matrix surrounding the crystallites. In addition, the dimensions of such crystallites surely come into play: the smaller their dimensions the more important are the surface effects. As a whole, we can envisage the formation of crystalline domains of large water and AHH-II clusters and much smaller regions of pure ammonia. This is in accordance with the composition of the loaded water/ammonia solution and with the spatial Raman analysis of the solid sample. The environmental

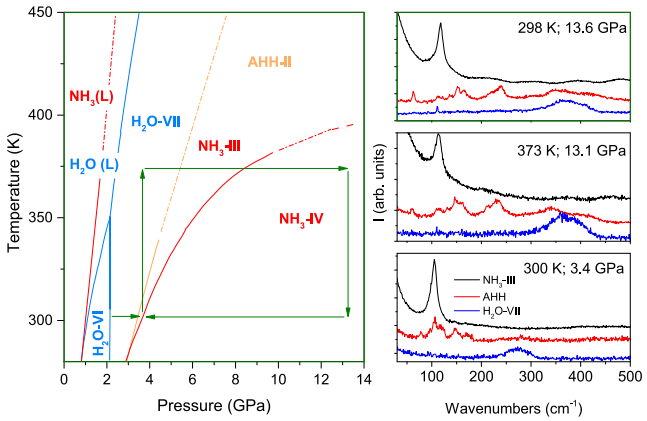

FIG. 12. Left: P–T path (green arrows) followed superimposed on the phase diagrams of NH_3[36] (red lines), H_2O[54] (blue lines), and AHH[55] (orange lines). Right: representative lattice phonon spectra of the three species measured along the path.

effects seem to be much larger on these smaller crystallites, which can give rise to non equilibrium structures resulting from kinetically controlled crystal transformations.

In this respect, the effect of increasing temperature can help to understand this behavior. First of all, thermal annealing facilitates the removal of metastabilities and structural defects, also favoring the dimensional growth of the crystallites. In addition, the increased amplitude of the molecular motions is effective in weakening or even destroying the H-bond network, thus representing a powerful tool to overcome the energetic barrier in order to access the thermodynamic stable phase or to allow a chemical transformation.[51–53] For this purpose, we have performed an experiment heating almost isobarically (3.5–3.9 GPa) the 2:1 water–ammonia mixture up to 375 K, where an isothermal compression to 13.6 GPa was performed. Throughout this P–T interval, Raman maps were recorded by mesh acquisition in steps of 4 or 10/12 μm to check whether the spatial distribution of the crystalline mixture changed in terms of species (NH_3, H_2O, and AHH) and dimensions of the crystalline domains.

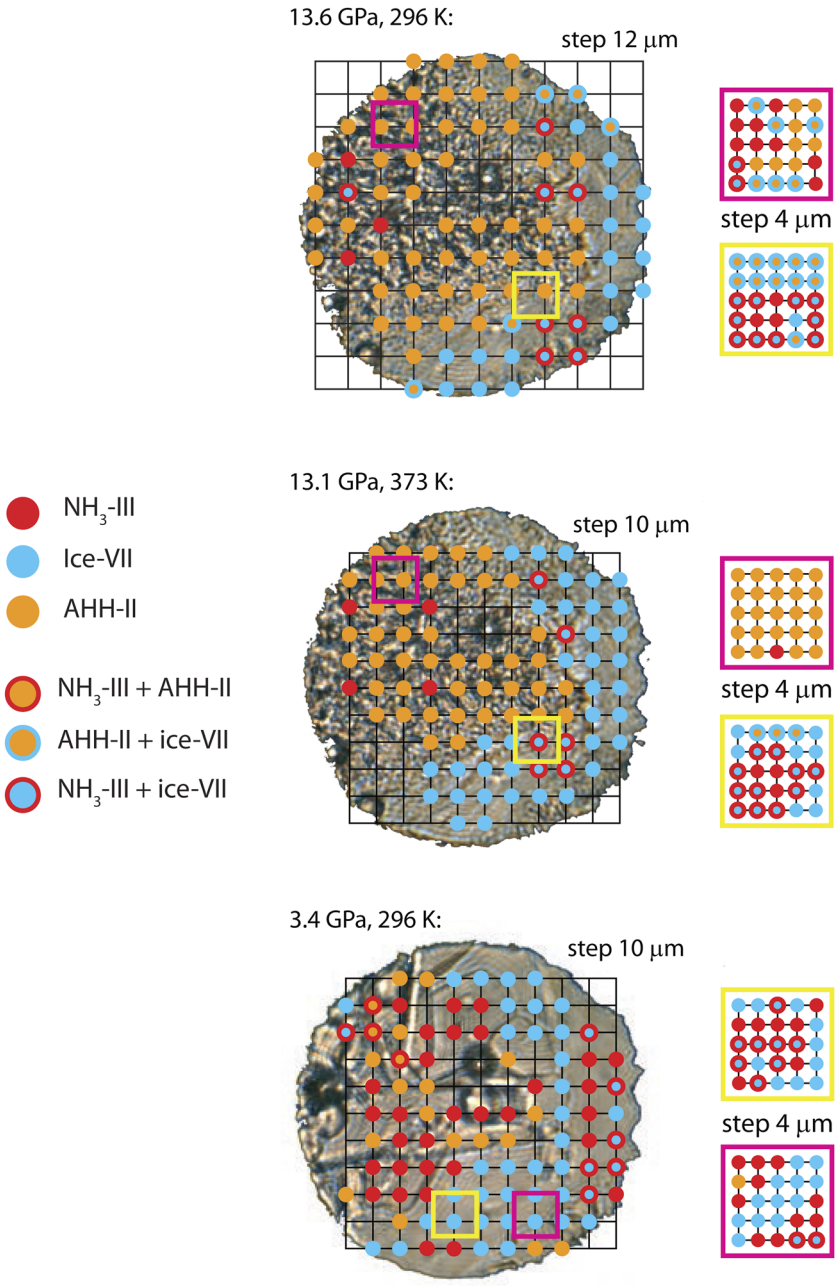

FIG. 13. Sample images acquired at different P–T conditions to which have been superimposed the grids formed by the points where the Raman spectra were acquired. These points have been colored according to the species identified through the spectra reported in Fig. 12, and the correspondence between colors and species is reported on the left side. P–T conditions and steps of the measurements are reported for each image. On the right side, we also report the Raman mesh acquired with a smaller step in specific regions of the sample identified by the colored boxes.

It is worth remembering that the spatial resolution of our system is about 3 μm, while the depth of focus is ≤10 μm.

In Fig. 12, we report the followed P–T path and representative lattice phonon spectra of the three crystallites present in the sample, NH_3-III, H_2O-VII, and AHH-II, measured at different P–T points along the path. The identification of the three species through these spectra is, therefore, straightforward, allowing us to draw the distribution map of the different species through the measurement of Raman mesh.

The detailed results of this analysis are reported for representative P–T points in Fig. 13. This analysis is interesting in different respects. Indeed, besides accounting for the spatial distribution of the different species, it reveals how this distribution remarkably changes when the acquisition step is modified. The spectra were measured in different regions both in steps of 10 or 12 μm (black mesh in Fig. 13) and in steps of 4 μm (colored boxes in Fig. 13). By comparing these measures, it is evident that areas with an apparent homogeneous distribution, according to the 10 or 12 μm steps meshes, actually reveal a considerably variable composition when the mesh step is decreased. Magenta and yellow boxes in the top (13.6 GPa and 296 K) and in the bottom (3.4 GPa and 296 K) are representative examples of the appearance of a more variable composition when the acquisition step is lowered to 4 μm. Unfortunately, this analysis cannot be pushed further because an additional reduction in the acquisition step would be limited by the spatial resolution, which is around 3 μm. Therefore, by these data, it is not possible to either support or rule out the possibility that the observed persistence of NH_3-III in the stability range of NH_3-IV, never observed in the solid mixture, is related to the reduced crystallites dimensions that, in combination with the strong H bonds with neighboring water molecules, prevent the structural rearrangement. In addition, a temperature increase of hundred degrees does not produce appreciable changes in the mixture composition and in the capability to characterize the extension of the crystallites, which is limited by the spatial resolution.

V. CONCLUSIONS

Water and ammonia are, together with methane, the main components of the molecular mixtures present in the interiors of Uranus and Neptune, and they are presumed to feature also in several recently discovered Neptune-like exoplanets. Going from the surface to the deep interior, these mixtures are exposed to a large gradient of both pressure and temperature and it is difficult to envisage how these ices are organized inside the planetary interior. Laboratory experiments have shown new compounds, unusual stoichiometries, and exotic crystal arrangements, which develop with increasing pressure on pure samples as well as on binary mixtures of the simplest molecular systems. Our understanding of these icy planets heavily relies on the modeling of the internal structural and dynamical properties, which is constrained by direct observations and by the aforementioned laboratory experiments. An additional motif of interest for the ammonia and water mixtures lies in the strongly hydrogen-bonded networks they can form in condensed phases and in the role that both N–H···O and O–H···N can assume upon compression as far as the structural rearrangements are concerned. This issue overcomes the boundaries of astrochemistry being, for example, responsible for supramolecular ordering in biological systems. Through the spectroscopic signature of the crystal structure, the lattice phonon spectrum, we have revealed a progressive hindering of the free rotation of the NH_3 molecules in phase III that gives rise to the activation of a librational Raman band above 2 GPa. This feature, and its intensification with pressure, is likely related, as already observed in nitrogen crystal, to a site symmetry lowering. Besides the structural information concerning the ammonia crystal, this phonon band allowed us to trace the quite complex and anomalous structural evolution with pressure of the mixture. The 2:1 H_2O:NH_3 mixture once subjected to P–T cycles always gives rise to the coexistence of segregated ice, ammonia, and AHH crystalline clusters. All of them behave differently with respect to the pure massive systems, exhibiting higher crystallization pressures ascribable to the more extreme conditions required for an fficient segregation of the mixture components to trigger the nucleation process. The missed observation of NH3-IV, replaced in its entire stability pressure range by NH3-III, could be related to surface effects due to the strong H-bonds. Indeed, H-bonds connect the surface's molecules to neighboring water molecules, making the structural rearrangement energetically costly and, thus, kinetically controlled.

ACKNOWLEDGMENTS

We thank the European Laboratory for Nonlinear Spectroscopy (LENS) for hosting the research and the Deep Carbon Observatory and the "Fondazione CR Firenze" for the strong support. This study was supported by the following grants: Extreme Physics and Chemistry of Carbon: Forms, Transformations, and Movements in Planetary Interiors funded by the Alfred P. Sloan Foundation; Fondazione Cassa di Risparmio di Firenze under the project "Dinamiche di fusione di ghiacci e idrati: accesso al regime mesoscopico."

AUTHOR DECLARATIONS

Conflict of Interest

The authors have no conflicts to disclose.

Author Contributions

Selene Berni: Data curation (equal); Formal analysis (equal); Investigation (equal); Methodology (equal); Writing – original draft (equal); Writing – review & editing (equal). **Demetrio Scelta**: Conceptualization (equal); Data curation (equal); Formal analysis (equal); Investigation (equal); Methodology (equal); Writing – original draft (equal); Writing – review & editing (equal). **Samuele Fanetti**: Data curation (equal); Formal analysis (equal); Investigation (equal); Methodology (equal); Writing – original draft (equal); Writing – review & editing (equal). **Roberto Bini**: Conceptualization (equal); Formal analysis (equal); Funding acquisition (equal); Supervision (equal); Writing – original draft (equal); Writing – review & editing (equal).

DATA AVAILABILITY

The data that support the findings of this study are available from the corresponding author upon reasonable request.

REFERENCES

[1]W. B. Hubbard and J. J. MacFarlane, J. Geophys. Res. **85**, 225, https://doi.org/10.1029/jb085ib01p00225 (1980).
[2]W. B. Hubbard, Science **214**, 145 (1981).
[3]M. Ross, Nature **292**, 435 (1981).
[4]T. Guillot, Science **286**, 72 (1999).
[5]O. G. Benvenuto, A. Fortier, and A. Brunini, Icarus **204**, 752 (2009).
[6]A. D. Fortes and M. Choukroun, Space Sci. Rev. **153**, 185 (2010).
[7]G. Tobie, D. Gautier, and F. Hersant, Astrophys. J. **752**, 125 (2012).
[8]A. G. Hayes, R. D. Lorenz, and J. I. Lunine, Nat. Geosci. **11**, 306 (2018).
[9]J. S. Loveday, R. J. Nelmes, M. Guthrie, S. A. Belmonte, D. R. Allan, D. D. Klug, J. S. Tse, and Y. P. Handa, Nature **410**, 661 (2001).
[10]M. Choukroun, O. Grasset, G. Tobie, and C. Sotin, Icarus **205**, 581 (2010).
[11]O. Grasset and J. Pargamin, Planet. Space Sci. **53**, 371 (2005).
[12]A. D. Fortes, Planet. Space Sci. **60**, 10 (2012).
[13]S. Schaack, U. Ranieri, P. Depondt, R. Gaal, W. F. Kuhs, P. Gillet, F. Finocchi, and L. E. Bove, Proc. Natl. Acad. Sci. U. S. A. **116**, 16204 (2019).
[14]D. Scelta, S. Fanetti, S. Berni, M. Ceppatelli, and R. Bini, J. Phys. Chem. C **126**, 19487 (2022).
[15]A. D. Fortes, E. Suard, M.-H. Lemée-Cailleau, C. J. Pickard, and R. J. Needs, J. Am. Chem. Soc. **131**, 13508 (2009).
[16]C. W. Wilson, C. L. Bull, G. Stinton, and J. S. Loveday, J. Chem. Phys. **136**, 094506 (2012).
[17]J. S. Loveday and R. J. Nelmes, Phys. Rev. Lett. **83**, 4329 (1999).
[18]C. W. Wilson, C. L. Bull, G. W. Stinton, D. M. Amos, M.-E. Donnelly, and J. S. Loveday, J. Chem. Phys. **142**, 094707 (2015).
[19]C. Liu, A. Mafety, J. A. Queyroux, C. W. Wilson, H. Zhang, K. Béneut, G. Le Marchand, B. Baptiste, P. Dumas, G. Garbarino, F. Finocchi, J. S. Loveday, F. Pietrucci, A. M. Saitta, F. Datchi, and S. Ninet, Nat. Commun. **8**, 1065 (2017).
[20]A. D. Fortes, J. P. Brodholt, I. G. Wood, L. Vočadlo, and H. D. B. Jenkins, J. Chem. Phys. **115**, 7006 (2001).
[21]G. I. G. Griffiths, A. J. Misquitta, A. D. Fortes, C. J. Pickard, and R. J. Needs, J. Chem. Phys. **137**, 064506 (2012).
[22]M. Bethkenhagen, D. Cebulla, R. Redmer, and S. Hamel, J. Phys. Chem. A **119**, 10582 (2015).
[23]H. Zhang, F. Datchi, L. M. Andriambariarijaona, G. Zhang, J. A. Queyroux, K. Béneut, M. Mezouar, and S. Ninet, J. Chem. Phys. **153**, 154503 (2020).
[24]H. Zhang, F. Datchi, L. Andriambariarijaona, M. Rescigno, L. E. Bove, S. Klotz, and S. Ninet, J. Phys. Chem. Lett. **14**, 2301 (2023).
[25]A. F. Goncharov, N. Goldman, L. E. Fried, J. C. Crowhurst, I.-F. W. Kuo, C. J. Mundy, and J. M. Zaug, Phys. Rev. Lett. **94**, 125508 (2005).
[26]M. Millot, S. Hamel, J. R. Rygg, P. M. Celliers, G. W. Collins, F. Coppari, D. E. Fratanduono, R. Jeanloz, D. C. Swift, and J. H. Eggert, Nat. Phys. **14**, 297 (2018).
[27]S. Ninet, F. Datchi, and A. M. Saitta, Phys. Rev. Lett. **108**, 165702 (2012).
[28]T. Palasyuk, I. Troyan, M. Eremets, V. Drozd, S. Medvedev, P. Zaleski-Ejgierd, E. Magos-Palasyuk, H. Wang, S. A. Bonev, D. Dudenko, and P. Naumov, Nat. Commun. **5**, 3460 (2014).
[29]V. N. Robinson, Y. Wang, Y. Ma, and A. Hermann, Proc. Natl. Acad. Sci. U. S. A. **114**, 9003 (2017).
[30]I. Lunine and D. J. Stevenson, Icarus **70**, 61 (1987).
[31]K. E. Mandt, O. Mousis, J. Lunine, and D. Gautier, Astrophys. J. Lett. **788**, L24 (2014).
[32]C. Ma, F. Li, Q. Zhou, F. Huang, J. Wang, M. Zhang, Z. Wang, and Q. Cui, RSC Adv. **2**, 4920 (2012).
[33]M. Gauthier, Ph. Pruzan, J. C. Chervin, and J. M. Besson, Phys. Rev. B **37**, 2102 (1988).
[34]J. S. Loveday, R. J. Nelmes, W. G. Marshall, J. M. Besson, S. Klotz, and G. Hamel, Phys. Rev. Lett. **76**, 74 (1996).
[35]S. Ninet, F. Datchi, A. M. Saitta, M. Lazzeri, and B. Canny, Phys. Rev. B **74**, 104101 (2006).
[36]S. Ninet and F. Datchi, J. Chem. Phys. **128**, 154508 (2008).
[37]S. Ninet, F. Datchi, S. Klotz, G. Hamel, J. S. Loveday, and R. J. Nelmes, Phys. Rev. B **79**, 100101 (2009).
[38]H. K. Mao, P. M. Bell, J. V. Shaner, and D. J. Steinberg, J. Appl. Phys. **49**, 3276 (1978).
[39]D. Scelta, M. Ceppatelli, R. Ballerini, A. Hajeb, M. Peruzzini, and R. Bini, Rev. Sci. Instrum. **89**, 053903 (2018).
[40]M. Ceppatelli, F. A. Gorelli, J. Haines, M. Santoro, and R. Bini, Z. Kristallogr. **229**, 83 (2014).
[41]D. D. Ragan, R. Gustavsen, and D. Schiferl, J. Appl. Phys. **72**, 5539 (1992).
[42]B. Minceva-Sukarova, W. F. Sherman, and G. R. Wilkinson, J. Phys. C: Solid State Phys. **17**, 5833 (1984).
[43]P. Pruzan, J. C. Chervin, and M. Gauthier, Europhys. Lett. **13**, 81 (1990).
[44]W. Xu, V. N. Robinson, X. Zhang, H.-C. Zhang, M.-E. Donnelly, P. Dalladay-Simpson, A. Hermann, X.-D. Liu, and E. Gregoryanz, Phys. Rev. Lett. **126**, 015702 (2021).
[45]R. B. Von Dreele and R. C. Hanson, Acta Crystallogr., Sect. C: Cryst. Struct. Commun. **C40**, 1635 (1984).
[46]P. Pruzan, D. H. Liebenberg, and B. I. Mills, Phys. Rev. Lett. **48**, 1200 (1982).
[47]R. Bini, M. Jordan, L. Ulivi, and H. J. Jodl, J. Chem. Phys. **108**, 6849 (1998).
[48]A. D. Fortes, I. G. Wood, L. Vocadlo, K. S. Knight, W. G. Marshall, M. G. Tucker, and F. Fernandez-Alonso, J. Appl. Cryst. **42**, 846 (2009).
[49]W. P. Hsieh and Y. H. Chien, Sci. Rep. **5**, 8532 (2015).
[50]L. Dougan, R. Hargreaves, S. P. Bates, J. L. Finney, V. Réat, A. K. Soper, and J. Crain, J. Chem. Phys. **122**, 174514 (2005).
[51]K. Dziubek, M. Citroni, S. Fanetti, A. B. Cairns, and R. Bini, J. Phys. Chem. C **121**, 2380 (2017).
[52]S. Fanetti, M. Citroni, K. Dziubek, M. M. Nobrega, and R. Bini, J. Phys.: Condens. Matter **30**, 094001 (2018).
[53]S. Fanetti, M. Santoro, F. Alabarse, E. Berretti, and R. Bini, Nanoscale **12**, 5233 (2020).
[54]A. K. Soper, Science **297**, 1288 (2002).
[55]A. D. Fortes, I. G. Wood, M. Alfredsson, L. Vočadlo, K. S. Knight, W. G. Marshall, M. G. Tucker, and F. Fernandez-Alonso, High Pressure Res. **27**, 201 (2007).